

The hydrothermal diamond anvil cell (HDAC) and its applications

WILLIAM A. BASSETT¹, TZY-CHUNG WU¹, I-MING CHOU², H. T. HASELTON², JR., JOHN FRANTZ³,
BJORN O. MYSEN³, WUU-LIANG HUANG⁴, SHIV K. SHARMA⁵, DAVID SCHIFERL⁶

¹Department of Geological Sciences, Snee Hall, Cornell University, Ithaca, NY 14853, U.S.A.

²MS 959 U.S. Geological Survey, Reston, VA 22092, U.S.A.

³Geophysical Laboratory, 5251 Broad Branch Rd. NW, Washington, DC 20015, U.S.A.

⁴Exxon Production Research Company, 3319 Mercer St. Houston, TX 77027, U.S.A.

⁵Hawaii Institute of Geophysics, University of Hawaii, 2525 Correa Rd., Honolulu, HI 96822, U.S.A.

⁶Materials Research, Los Alamos National Laboratory, Los Alamos, NM 87545, U.S.A.

Abstract—A new style of diamond anvil cell, which is called the hydrothermal diamond anvil cell (HDAC), has been developed to make accurate measurements on samples under pressure and at temperatures between -190°C and $+1200^{\circ}\text{C}$. It is especially suitable for fluid samples and for observing reactions between solids and fluids. The techniques for making observations and determinations used to date include optical microscopy, x-ray diffraction, Raman spectroscopy, luminescence, and infrared absorption. Three studies described in this paper deal with pressure-temperature calibration. They are (1) H_2O equation of state, (2) rapidly reversible second order phase transitions, and (3) shift of the Raman spectrum of diamond. Three applications of the HDAC described here include (1) luminescence and infrared absorption analyses of kerogen, lignite, and crude oil, (2) Raman spectroscopy of silicate melts, and (3) x-ray diffraction studies of dehydration and rehydration of montmorillonites using synchrotron radiation.

INTRODUCTION

THE HYDROTHERMAL diamond anvil cell (HDAC) is a new style of diamond anvil cell that was designed and built to meet a specific set of requirements (BASSETT *et al.*, 1993). It has been used to subject samples to a very uniform ($\pm 0.5^{\circ}\text{C}$) temperature over the range from -190 to $+1200^{\circ}\text{C}$, hold the temperature constant within $\pm 2^{\circ}\text{C}$, and measure the temperature by thermocouple with an accuracy of $\pm 1.5^{\circ}\text{C}$. A rhenium gasket properly prepared is capable of holding a constant volume within $\pm 2\%$ or better over most of the temperature range. If a fluid such as water is used as the sample or pressure medium, its equation of state can be used to determine the pressure from the measured temperature. When the equation of state is well known and the density of the fluid is accurately measured by homogenization temperature or freezing temperature, the accuracy of such pressure measurements is significantly greater than by other pressure measuring methods formerly used with diamond anvil cells. This and two other new pressure measuring techniques are described in this paper.

Optical microscopy can be used to make direct *in-situ* observations of changes in the solid, liquid, and vapor phases of a sample as a function of pressure and temperature. Raman spectroscopy, luminescence, infrared absorption, x-ray diffraction, as well as other techniques can also be used for making *in-situ* observations in the new diamond anvil cell. In this paper we describe some new

results from these techniques applied to a variety of samples held at high pressures and temperatures in the HDAC.

THE HYDROTHERMAL DIAMOND ANVIL CELL (HDAC)

Until recently, very few studies of hydrothermal reactions or of equations of state of fluids had been made in the diamond anvil cell (*e.g.*, VAN VALKENBURG *et al.*, 1987). The hydrothermal diamond anvil cell (HDAC), which is described in detail by BASSETT *et al.* (1993), consists of two platens with diamond anvils and heaters mounted at their centers (Fig. 1). The two platens are drawn together by tightening three nuts, thus applying pressure to a sample held between the diamond anvils. Samples are typically placed in a rhenium gasket consisting of a hole 200 to 500 μm in diameter and 75 to 500 μm thick. A rocker under one anvil allows for orientational alignment and a sliding disk under the other allows for translational alignment. Holes through the centers of the platens allow access to the sample for viewing and for various forms of electromagnetic radiation. Molybdenum wires wrapped around the tungsten carbide seats which support the diamond anvils serve as heaters (Fig. 2). These can heat the anvils and the sample very uniformly and very constantly to temperatures as high as 1200°C . By introducing liquid nitrogen the temperature can be reduced to -190°C . Electrical leads for the heaters and the thermocouples are fed through the platens. The vol-

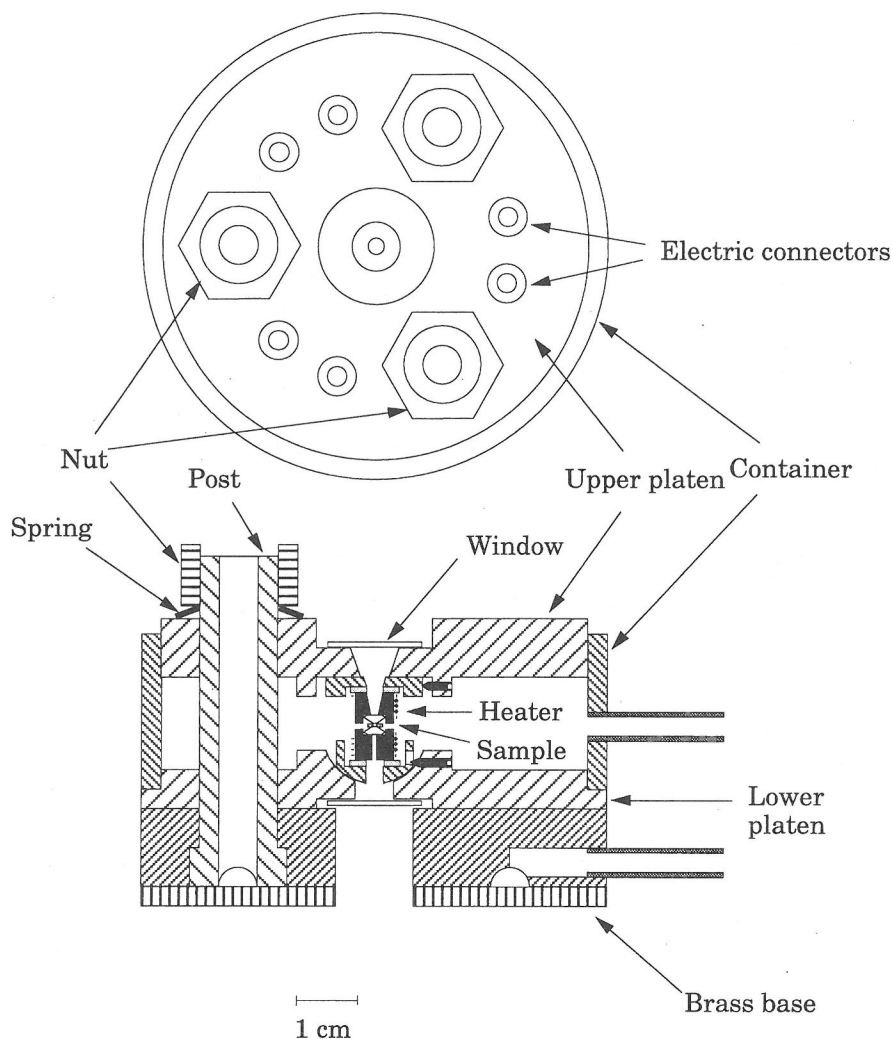


FIG. 1. Plan and elevation of the new diamond anvil cell. The diameter of the cell is 7.62 cm. The height is 5.72 cm. The base is constructed of brass; the platens, posts, and cylinder are constructed of stainless steel.

ume containing the heaters, the anvils, and the sample can be enclosed and completely surrounded with a gas to prevent oxidation. We have found that a constant flow of a mixture of Ar with 1% H_2 is very satisfactory for this purpose.

Laser light with any wavelength in the visible spectrum can be introduced into the top of the diamond cell to produce interference fringes in the sample chamber as well as the solid samples. Interference fringes produced by laser light reflected from top and bottom anvil faces provide a means for monitoring the volume of sample chamber. This is made possible by assuming that the refractive index of the homogeneous fluid portion of the sam-

ple remains constant during isochoric experiments. Fringes produced by laser light reflected from the top and bottom of a doubly polished solid sample provide a very sensitive means for observing volume and refractive index changes in samples due to transitions and reactions.

PRESSURE MEASUREMENT BY EQUATION OF STATE OF A FLUID AND HYDROTHERMAL STUDIES USING VISUAL OBSERVATION

When a sample is loaded in a gasketed diamond anvil cell surrounded by a fluid of known equation of state such as water, the pressure at which an

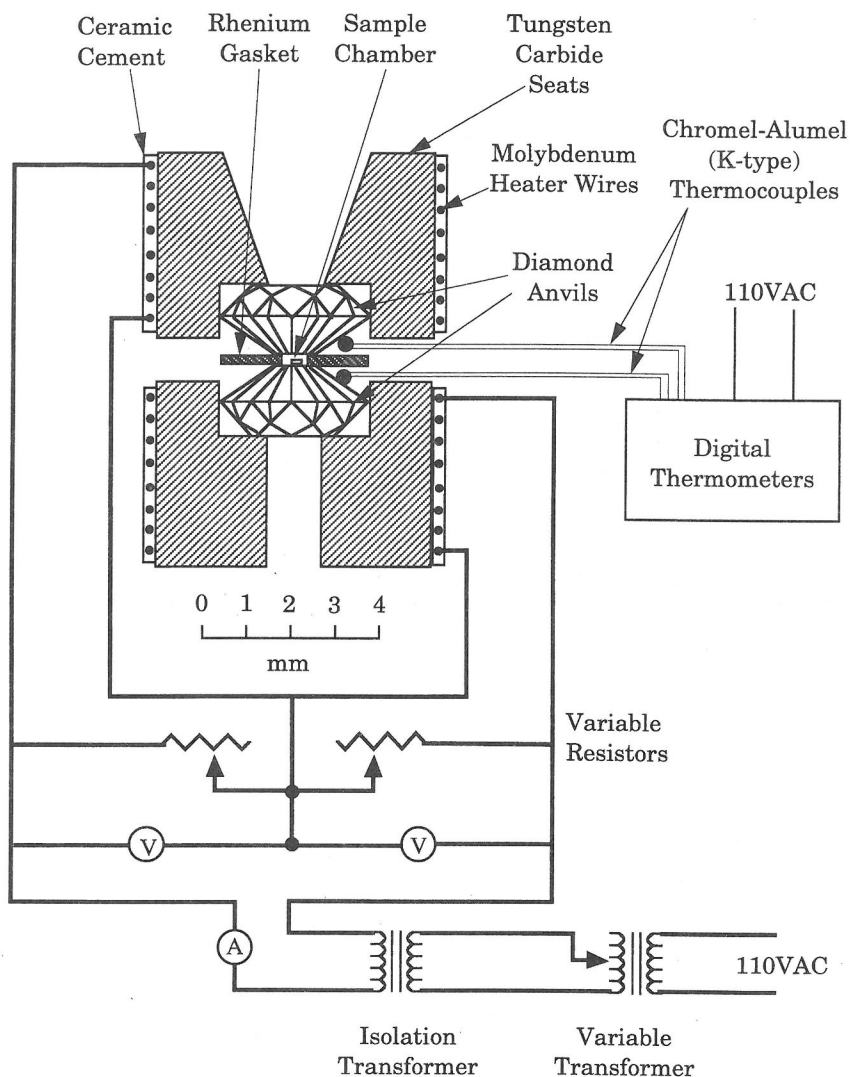


FIG. 2. Schematic diagram showing details of the sample, diamond anvils, heaters, and the electric circuits for heating, controlling, and measuring the temperature of the sample.

observation is made can be ascertained by the following steps: (1) determine the density of the fluid by measuring the temperature of a suitable transition such as homogenization or melting using the equation of state or P-T- ρ diagram of the fluid (Fig. 3); (2) monitor the sample chamber size to see that it does not change significantly by observing interference fringes caused by reflected laser light from the upper and lower anvil faces; (3) measure the temperature at which you make an observation on your sample; (4) using the equation of state or P-T- ρ diagram of the fluid, solve for the pressure. In practice the most accurate results are obtained

during the cooling part of the cycle during which there is much less change of the gasket thickness. The path that is typically followed through the P-T- ρ diagram is illustrated in Fig. 4.

Independent Check of the Equation of State of H₂O

At Cornell University we have used the HDAC to compare the equation of state of H₂O with the P-T boundary of the α - β transition in quartz. The sample for these experiments consisted of a doubly-polished quartz platelet, distilled, deionized water, and an air

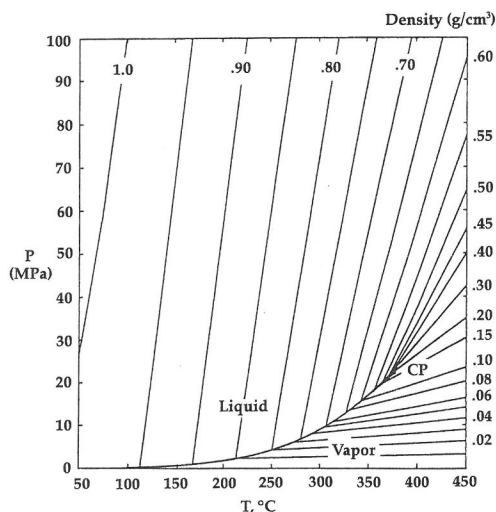


FIG. 3. Pressure-temperature plot of the equation of state of H_2O . LV represents the liquid-vapor coexistence curve and CP represents the critical point. The isochores are labeled by density (ρ) in g/cm^3 .

bubble (Fig. 5). The sample was then heated until the bubble disappeared (homogenization). As the sample was further heated, both the temperature and pressure of the homogeneous fluid increased. This was continued until sudden motion of interference fringes was observed indicating the α - β transition. The sample was then cooled until a vapor bubble reappeared. If the interference fringes produced by reflection from the upper and lower anvil faces and the outline of the chamber hole indicated insignificant change during cooling, the volume of the sample chamber was assumed to have remained constant and, therefore, to have been isochoric. The sample was then slowly reheated until the vapor bubble disappeared, and the temperature at the moment of bubble disappearance was measured. If there was no loss of fluid during the experiment, this new homogenization temperature is typically found to be lower than the starting homogenization temperature indicating an increase in density due to relaxation of the gasket during the heating. The isochore density was determined from this homogenization temperature and the transition pressure was determined from the temperature along the isochore at the time fringe movement in the quartz was observed. Our results (SHEN *et al.*, 1992) show that the equation of state of H_2O of HAAR *et al.* (1984) is in good agreement with the α - β quartz boundary of MIRWALD and MASSONNE (1980) for several different isochores.

Isochores of increasing density were studied this way until temperatures required were so high that

rapid solution of the quartz crystal took place before the α - β transition in the quartz could be observed. These techniques are described in more detail in BASSETT *et al.* (1993) and SHEN *et al.* (1992).

Precision and Accuracy

The thermocouples are not subject to any pressure-induced error because they are external and therefore not pressurized. Temperature can be measured with a precision of $\pm 0.1^\circ\text{C}$ over the range of temperature from -110°C to 380°C . The accuracy of our measurements is $\pm 0.5^\circ\text{C}$ over the same range. At temperatures from -190°C to -110°C and above 380°C , the precision is $\pm 0.5^\circ\text{C}$ and the accuracy is $\pm 1.5^\circ\text{C}$.

The accuracy of a pressure determination depends on the accuracies of the temperature measurements and the equation of state of H_2O (Fig. 3) or other fluid being used as pressure medium. The accuracy for our homogenization temperature measurements in H_2O is believed to be $\pm 0.5^\circ\text{C}$, which corresponds to a maximum density uncertainty of ± 0.004 (g/cm^3). When all of the uncertainties are collected, this method is considered to provide pressure determinations with an accuracy of 1% in the range of temperatures and pressures up to 1000°C and 0.5 GPa respectively.

NEW SOLID PRESSURE CALIBRANTS USING VISUAL OBSERVATION

Three new pressure calibrants have been characterized in the HDAC using H_2O as the pressure medium. They are BaTiO_3 (CHOU *et al.*, 1993), $\text{Pb}_3(\text{PO}_4)_2$ (CHOU and NORD, 1994) and PbTiO_3 (CHOU and HASELTON, 1994), and their applicable temperature ranges are below about 120, 180, and 490°C , respectively (Fig. 6). The common features for these calibrants include: (1) they are all based on ferroelastic phase transitions that are rapid and can be easily and precisely determined visually; (2) the transition temperatures decrease as pressure increases, such that the phase boundaries in P-T space intersect isochores of common geologic fluids at high angles (Fig. 6) and, thus, facilitate their application; and (3) that they are inert in most pressure media in a wide P-T range.

To apply these calibrants in the HDAC, a doubly polished platelet or a cleavage fragment (typically $200 \times 200 \times 40 \mu\text{m}$) is loaded with a fluid pressure medium in the HDAC. The tetragonal-cubic phase transition for BaTiO_3 and the monoclinic-trigonal transition for $\text{Pb}_3(\text{PO}_4)_2$ can both be detected by the disappearance and reappearance of twin boundaries during heating and cooling, respectively. The hysteresis is less than

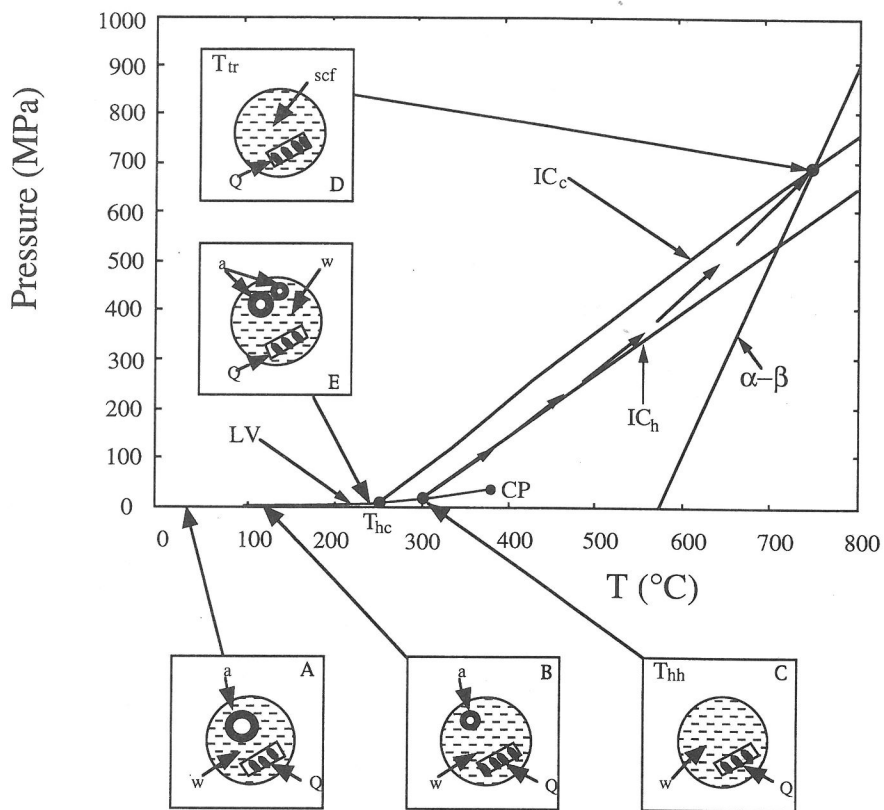


FIG. 4. This diagram shows a typical pressure-temperature path of an experiment to examine the α - β transition in quartz. Insets show the appearances of the sample chamber at various steps along the path. CP is the critical point, LV is the liquid-vapor coexistence curve, IC_h is the isochore followed during heating, IC_c is the isochore followed during cooling, T_{hh} is the homogenization temperature during heating, T_{hc} is the homogenization temperature during cooling, T_{tr} is the transition temperature, a is an air bubble, w is water, scf is supercritical fluid, Q is a sample of quartz. The steep straight line represents the α - β transition in quartz.

1°C and 0.2°C for $BaTiO_3$ and $Pb_3(PO_4)_2$, respectively. We can determine the transition temperatures (T_{tr}) with a precision of $\pm 0.2^\circ C$ and an accuracy of $\pm 0.5^\circ C$. The tetragonal-cubic phase transition in $PbTiO_3$, which is indicated by the movements of phase fronts, was detected optically at a heating or cooling rate of about $1^\circ C/min$. The temperature interval in which the phase transition occurs ranges from $0.8^\circ C$ to $2.8^\circ C$, depending on pressure. The temperature at which the movement of phase fronts starts (or ends) on heating (or cooling) is taken as the transition temperature [$T_{tr,h}$ (or $T_{tr,c}$)]; these temperatures can be determined with a precision of $\pm 0.4^\circ C$ and an accuracy of $\pm 1.5^\circ C$. Results of our calibration are shown in Fig. 6 and described in the following sections.

$BaTiO_3$

Different regions of our $BaTiO_3$ sample, synthesized by MATTHIAS (1948) and characterized by

EVANS (1961), have different T_{tr} values (113-120°C at 1 atm.); these differences may be due to variations in impurity content or local strain. For a specific region of the crystal in our heating experiments, we observed $T_{tr} = 115.3^\circ C$ at 0.17 MPa (1.7 bar) along the liquid-vapor curve of pure H_2O (SAUL and WAGNER, 1989) and $49.2^\circ C$ at 1404.8 MPa (14048 bar) along the ice VI-water boundary (WAGNER *et al.*, 1994). On the basis of these measurements, we obtained the relation

$$P_{tr}(\text{MPa}) = 0.17 - 21.25 [(T_{tr})_P - (T_{tr})_{LV}] \quad (1)$$

where LV represents the liquid-vapor pressure of pure H_2O . Observations at intermediate pressures, when compared with H_2O equation of state calculations, are consistent with a linear relationship. The slope of $-21.25 \text{ MPa}/^\circ C$ ($-212.5 \text{ bar}/^\circ C$) agrees very well with the value reported by SAMARA

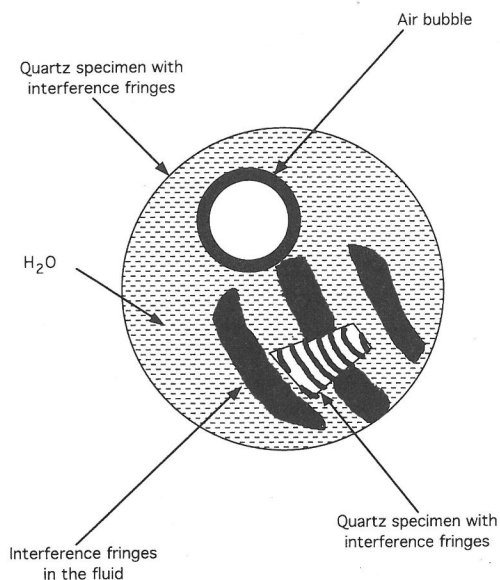


FIG. 5. Typical appearance of a solid sample in liquid water with an air bubble in a circular rhenium gasket hole 500 μm in diameter. The portion of the sample illuminated with laser light shows coarse fringes due to interference between light reflected from the two anvil faces. The fine fringes in the solid quartz sample are caused by interference between light reflected from the top and bottom of the platelet.

($-21.0 \text{ MPa}/^\circ\text{C}$ with $(T_{tr})_{0.1 \text{ MPa}} = 122^\circ\text{C}$ ($-210 \text{ bar}/^\circ\text{C}$ with $(T_{tr})_{1 \text{ bar}} = 122^\circ\text{C}$) cited in RAMIREZ *et al.* (1990). The data of DECKER and ZHAO (1989) indicate that the equation given above is probably valid to the tricritical pressure for BaTiO_3 of about 3.5 GPa (35 kbar).

$\text{Pb}_3(\text{PO}_4)_2$

In our heating experiments, the monoclinic-trigonal transition occurs at 180.2°C and 1.01 MPa (10.1 bar) along the L-V curve of H_2O and at 49.1°C and 1402.7 MPa (14027 bar) along the ice VI and water boundary. These two P-T points define a linear phase boundary having a slope of $-10.62 \text{ MPa}/^\circ\text{C}$ ($-106.2 \text{ bar}/^\circ\text{C}$). Observations at intermediate pressures (along several isochores of H_2O), when combined with H_2O equation of state calculations, are consistent with this linear relation. Our measured T_{tr} value agrees very well with the value of 180.4°C at 1 atm. reported by BISMAYER and SALJE (1981). This calibrant has a pressure resolution of $\pm 2.1 \text{ MPa}$ (21 bar), which is twice the sensitivity of BaTiO_3 described above.

PbTiO_3

The sample used in our calibration experiments was synthesized and characterized by BING-NAN SUN (personal communication, 1994). The tetragonal-cubic phase transition temperatures were determined at 1 atm. and along six isochores of H_2O in our heating and cooling experiments (CHOU and HASELTON, 1994). Least squares regression of our data give

$$P_{tr,h}(\text{MPa}) = 7021.7 - 14.235 T_{tr,h}(\text{C}), \quad (2)$$

$$P_{tr,c}(\text{MPa}) = 6831.3 - 14.001 T_{tr,c}(\text{C}), \quad (3)$$

with the R-squared values of 0.9966 and 0.9987, respectively. For clarity, only the first equation is plotted in Fig. 6. The slopes for the phase boundary are -14.235 and $-14.001 \text{ MPa}/^\circ\text{C}$ (-142.35 and $-140.01 \text{ bar}/^\circ\text{C}$), respectively. They are more negative than the $-11.91 \text{ MPa}/^\circ\text{C}$ ($-119.1 \text{ bar}/^\circ\text{C}$) reported by SAMARA (1971) for uranium-doped PbTiO_3 ; the variation may result from the compositional difference.

RAMAN SPECTROSCOPY OF ^{13}C DIAMOND AS PRESSURE SENSOR AT HIGH TEMPERATURES: MELT STUDIES OF HYDRATED SILICATES

Raman spectroscopy of ^{13}C diamond has been developed as a new method for measuring pressure

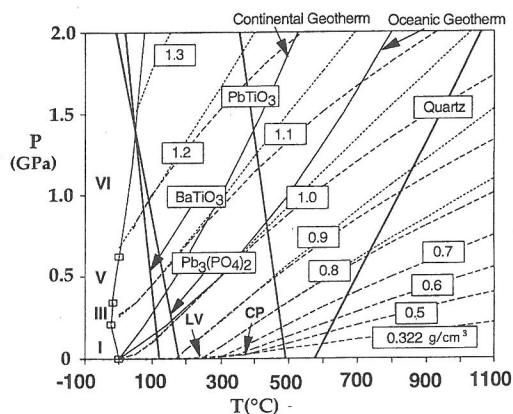


FIG. 6. A P-T plot showing the phase relations in pure H_2O and four pressure calibrants (quartz, PbTiO_3 , $\text{Pb}_3(\text{PO}_4)_2$, and BaTiO_3). I, III, V, and VI are ice polymorphs; LV is the liquid-vapor curve of H_2O ; CP is the critical point of H_2O ; the long dashed and dotted curves are isochores of H_2O derived from equations of state formulated by HAAR *et al.* (1984) and SAUL and WAGNER (1989), respectively. The numbers in the rectangles give the densities of the isochores in g/cm^3 .

at high temperatures in diamond anvil cells (SCHIFERL *et al.*, in preparation). When combined with Raman spectroscopy of ^{12}C diamond, the method becomes a powerful means for measuring pressure at high temperatures, especially in samples that are corrosive to oxide pressure sensors such as ruby and Sm:YAG.

At the University of Hawaii, experiments are being conducted at simultaneous high P and T conditions in diamond anvil cells for studying minerals and hydrated silicate melts. The HDAC style of cell as well as an externally heated Merrill-Bassett DAC have been adapted for use with a multichannel micro-Raman spectrometer with a fiber-optics based technique to acquire pressure sensitive fluorescence spectra of Sm:YAG simultaneously with Raman spectra of the sample. High-frequency Raman spectra of forsterite have been measured to 650°C (923 K) and pressures above 8 GPa (80 kbar) (SCHIFERL *et al.*, 1993).

The HDAC is easily mounted on the stage of the Raman microscope for optical observation and Raman spectral measurements of samples pressurized to 10 GPa (100 kbar) and simultaneously heated to 900°C (1173 K). With the HDAC we measured Raman spectra of hydrous potassium silicate and hydrous albite to 10 GPa (100 kbar) at room temperature. We have also measured spectra of hydrous potassium silicate melts to 550°C (823 K) and at pressures of about 0.7 GPa (7 kbar) but encountered technical difficulties. One of the major problems with hydrous silicate systems is that these are extremely corrosive, even at moderate temperature, and would invariably react with either ruby or Sm:YAG pressure calibrants. Furthermore, silicate glasses and melts are very weak Raman scatterers. In order to overcome these technical difficulties, we have refined the confocal micro-Raman technique so that it can be used with diamond anvil cells for recording spectra of very weak Raman scatterers (SHARMA *et al.*, 1994), and developed the $^{13}\text{C}/^{12}\text{C}$ diamond Raman sensor system for measuring pressure for all samples under any simultaneous P-T conditions that can be achieved in externally heated diamond-anvil cells (SCHIFERL *et al.*, in preparation).

The use of the Raman spectra of natural diamond (99% ^{12}C and 1% ^{13}C) for measuring pressure has been suggested by a number of authors (SHERMAN, 1985; HANDFLAND *et al.*, 1985; SHARMA *et al.*, 1985; ALEKSANDROV *et al.*, 1987; TARDIEU *et al.*, 1990). However, even with the micro-Raman technique it is very difficult to separate the Raman spectrum of the sensor chip from the strong Raman signal of diamond anvils both of which appear at

1332.5 cm^{-1} under ambient conditions. This problem persists to pressures above 14 GPa (140 kbar), where the Raman signal from the sensor chip under hydrostatic pressure moves (at $2.90 \pm 0.05 \text{ cm}^{-1}/\text{GPa}$) higher and becomes well separated from the Raman signals of the anvils.

We have used the HDAC as well as the Merrill-Bassett and Mao-Bell cells for measuring pressure dependence of the first-order Raman line of synthetic ^{13}C -enriched (91 atomic %) diamond film. The pressure dependence of the spectra of small ($20 \mu\text{m} \times 20 \mu\text{m} \times 20 \mu\text{m}$) fragments of the polycrystalline diamond film was measured with ruby R_1 and R_2 fluorescence, using either methanol-ethanol (4:1) mixture or water as pressure transmitting medium. At room temperature, 23°C (296 K), the Raman line of the ^{13}C -enriched film appears at 1287.79 cm^{-1} , and a fit of our data and that of MUNIOV *et al.* (1994) for the same ^{13}C diamond film yields a shift of $2.8294 \pm 0.047 \text{ cm}^{-1}/\text{GPa}$ (SCHIFERL *et al.*, in preparation). The temperature dependence of the Raman line of the ^{13}C diamond has been measured to 1056°C (1329 K) and is given by:

$$V(T) = 1294.5 - 0.022 T - 3.8 \times 10^{-6} T^2, \quad (4)$$

where V is the frequency in cm^{-1} and T is the temperature in Kelvin ($\text{K} = ^\circ\text{C} + 273.13$). Using these calibrations, the ^{13}C -diamond chip provides the first means of measuring pressure up to 16 GPa (160 kbar) accurately ($\pm 0.3 \text{ GPa}$ or $\pm 3 \text{ kbar}$) at temperatures as high as 927°C (1200 K) for samples in corrosive environments. Above 14 GPa (140 kbar), the Raman spectrum from the ^{12}C diamond chip under hydrostatic pressure comes out from under the diamond-anvil Raman line. Recently, the temperature dependence of the Raman line of natural diamonds has been measured to 1627°C (1900 K) (HERCHEN and CAPPELLI, 1991; ZOUBOULIS and GRIMSDITCH, 1991). The $^{13}\text{C}/^{12}\text{C}$ Raman pressure sensor system is now ready for measuring simultaneous high temperature and high pressure samples in diamond anvil cells.

IN SITU MONITORING OF ORGANIC TRANSFORMATION USING LUMINESCENCE AND FTIR SPECTROSCOPY

In the research lab of the Exxon Production Research Company we have developed techniques to monitor *in situ* organic transformation using visual observation, fluorescence, and infrared spectroscopy. The responses of organic materials to heating were observed in real-time using a microscope

equipped with a charge couple device (CCD) video monitoring system, and fluorescence was monitored using a luminescence spectrometer. Progressive changes of functional groups were monitored during transformation by micro-fourier transform infrared spectroscopy (micro-FTIR). Each spectrum accumulated from 50 scans was recorded with a spectral resolution of 4 cm^{-1} in the $700\text{--}4000\text{ cm}^{-1}$ range. Experiments were conducted in open and closed systems at anhydrous or hydrous conditions for kerogen, lignite, and crude oil samples. The merit of the HDAC over conventional hot-stage methods is its capability of conducting experiments at hydrous and high-pressure conditions. Preliminary results illustrate the capabilities of the technique to examine reaction pathways and the timing and rates of organic transformations. The visual experiments provide direct observations and estimations of the temperature (or timing) and yields of liquid and gas generation at a variety of experimental conditions.

Pyrolysis of kerogen

A concentrated kerogen from shale of the Green River Formation (Eocene) was heated at a rate of $25^\circ\text{C}/\text{min}$ to 380°C . The temperature was then held at 380°C for 118 hours. The results show a successive change in spectrum distribution in the range of 1700 to 3100 cm^{-1} . Deconvolution of the spectrum in this range using curve fitting has been performed to calculate five aliphatic C-H_x stretching bands ($\text{CH}_3(\text{asym})$, $\text{CH}_2(\text{asym})$, CH , $\text{CH}_3(\text{sym})$ and $\text{CH}_2(\text{sym})$) and one aromatic C-H stretching band. The dramatic increase in the $\text{CH}_3(\text{asym})/\text{CH}_2(\text{asym})$ intensity ratio of asymmetric aliphatic stretching bands at the late stage of pyrolysis indicates that the cleavage of aliphatic chains occurs during the kerogen transformation (LIN and RITZ, 1993). The trend of the aromatic/aliphatic stretching band ratio, which first increases then dramatically decreases, is probably attributable, respectively, to the formation of the alkyl-substituted aromatic hydrocarbons and the rapid cracking of aliphatic chains in the aromatic compounds at the late stage of pyrolysis (BENKHEDDA *et al.*, 1992). This preliminary study shows that in situ FTIR spectroscopic analysis during HDAC experiments has a potential to monitor the reaction pathways or derive kinetic information during kerogen transformation.

Cracking of crude oil

A crude oil sample from Gwydr Bay (API gravity = 31) was heated to 450°C at a rate of $25^\circ\text{C}/$

min. The temperature was then held at 450°C for 45 minutes. The results show that (1) a progressive decrease in the absorption band ratio of carbonyl or carboxyl C=O stretching ($\sim 1710\text{ cm}^{-1}$) to aromatic C=C stretching ($\sim 1630\text{ cm}^{-1}$); (2) the peak intensities for both aliphatic and aromatic groups progressively decrease with maturity, suggesting the cracking of oil to gas; (3) the aliphatic/aromatic band ratio ($1460\text{ cm}^{-1}/1630\text{ cm}^{-1}$) increases significantly (about two-fold) during the early and middle stages of maturation then decreases slightly with increasing maturity; (4) the methane absorption band at $\sim 3020\text{ cm}^{-1}$ was detected by probing the bubble space of the sample during cooling. The progressive variation of the functional groups in the samples during pyrolysis suggests that FTIR spectra can be used to follow the kinetics of oil cracking.

Monitoring timing of gas generation during pyrolysis of coals

A low maturity coal (lignite with vitrinite reflectance (Ro) = 0.31 and hydrogen index (HI) = 130) was heated at a rate of $25^\circ\text{C}/\text{min}$. to 380°C and the temperature was then held for 22 hours before cooling. The vapor generated within the sample chamber has been probed. The vapor species were identified from their designated functional groups. The results (Fig. 7) show that gas generation occurring from early to late follows the sequence: CO_2 , carbonyl-carboxylate vapors, hydroxyl-vapor, hydrocarbon wet gases and carbon monoxide. This technique can be an effective tool for studying the timing of generation of gases from source rocks. This technique is particularly useful for identifying the type of coals or kerogens which can thermally generate hydrocarbon gases at low maturity levels or for quantifying the effect of geological catalysts on generating premature gases from coals or kerogens.

ION-PAIRING IN MgSO_4 SOLUTIONS BY RAMAN SCATTERING

Gaskets lined with platinum were used to contain chemically reactive samples of MgSO_4 (FRANTZ *et al.*, 1994). A 0.5 m solution of MgSO_4 was analyzed using a micro-Raman spectrometer while conditions were changed along an isochore from room temperature to 500°C and 1.1 GPa (11 kbar). Relative abundances of species and the extent of ion pairing of MgSO_4 were measured along an isochore of $\sim 1\text{g}/\text{cm}^3$. Ion pairing was observed to increase with increasing pressure and the mass-action constants for the reaction $\text{Mg}^{+2} + \text{SO}_4^{2-}$

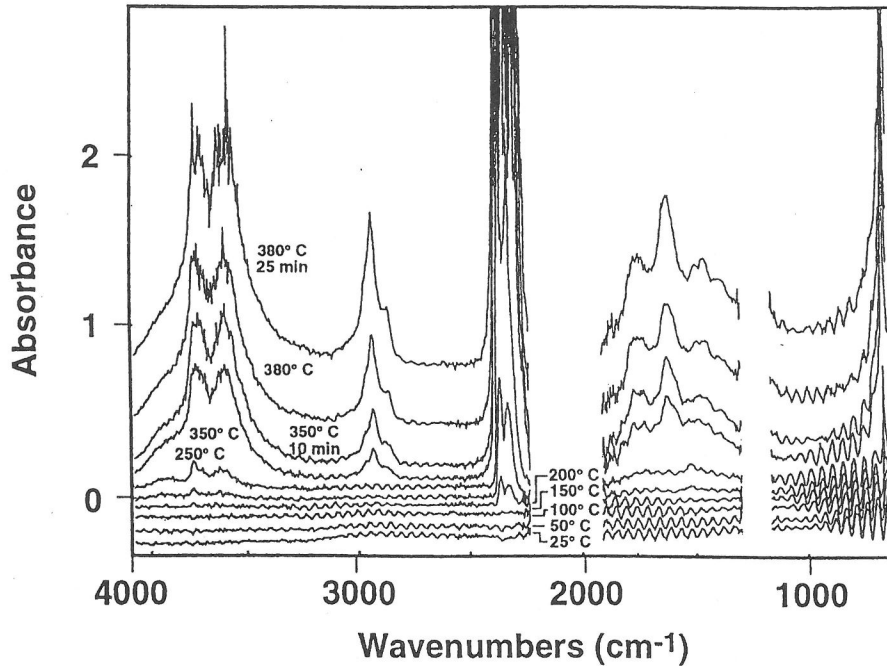


FIG. 7. Infrared spectra showing the generation of CO_2 , carbonyl-carboxylate vapors, hydroxyl-vapor, hydrocarbon wet gases and CO during heating of a lignite sample.

= MgSO_4 were found to range from 35 at 20°C and 0.1 MPa (1 bar) to 1.25×10^4 at 500°C and 1.14 GPa (11.4 kbar). These results are in good agreement with those obtained by RITZERT and FRANCK (1968) using electrical conductance measurements.

This trend of MgSO_4 to become a weaker electrolyte under hydrothermal conditions indicates a greater disruption of the relatively weak ion-water dipole bonds thus allowing a higher frequency of ion-ion interactions that result in ion pairing. This study of the effect of pressure and temperature on ion-water dipole bonds provides information that helps us to better understand viscosity as a function of pressure and temperature, a relationship that plays an important role in heat and mass transfer in the Earth's crust and mantle by flow of aqueous fluids.

HYDRATION AND DEHYDRATION OF CLAYS USING SYNCHROTRON RADIATION

The montmorillonite members of the clay family of minerals contain large quantities of water and are abundant in sediments. Therefore, they are among the most important hydrous phases to understand. These are sheet silicates with low nega-

tive charges on the sheets, charges that are balanced by cations filling the spaces between the sheets. Because of the low charges only a small number of cations fill the spaces and when they fill the spaces, they carry with them envelopes of H_2O molecules. These H_2O molecules reside between the sheets forming layers of water resulting in d-spacings along the c-axis of 12.5\AA , 15\AA , and 19\AA . These cations and their accompanying water molecules are readily exchanged when other cations are made available in solution.

Combining the HDAC with the very intense synchrotron radiation available on the white x-ray beamline at the Cornell High Energy Synchrotron Source (CHESS) has enabled us to make real-time measurements of changes in the hydration states of montmorillonites in response to changes in pressure and temperature. The sample consists of a grain of montmorillonite, distilled H_2O , and an air bubble. Pressure can be determined from the equation of state of the water as described in an earlier section. Energy dispersive x-ray diffraction patterns of our sample were obtained by passing a white beam of x-rays through the diamond anvils as the sample was heated and compressed. X-rays diffracted by our sample were collected by an intrinsic germanium detector placed at a 2θ angle of

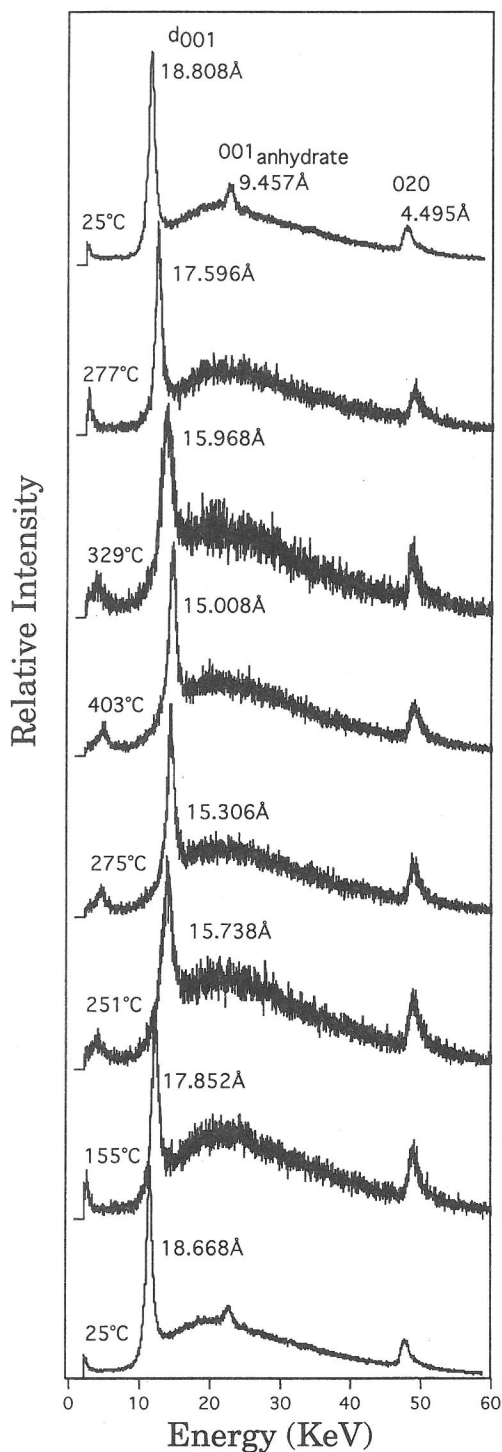


FIG. 8. A series of diffraction patterns of Ca-montmorillonite as the sample is heated and then cooled along the 1.053 g/cm^3 isochore.

3° (Fig. 8). Less than a minute was required to collect enough information to measure d-spacings. This allows us not only to observe the changes in the hydration states of water but also the response rate when temperature and pressure are changed. The three prominent hydration states of montmorillonite are easily recognized from the c-axis d-spacings.

Dehydration and rehydration experiments have been performed on montmorillonite with Ca, Mg, and Na cations in the exchange positions. Our results show that the 19\AA hydrate is stable up to $200\text{--}380^\circ\text{C}$ when the water pressure is greater than that along the H_2O liquid-vapor (LV) curve. The 15\AA hydrate is stable up to $450\text{--}600^\circ\text{C}$. At pressures greater than the LV curve the dehydration temperatures are not very sensitive to pressure but are sensitive to the interlayer cation species (Fig. 9). Increasing ionic potential (charge/radius) is correlated with a decrease in the temperature of the 19\AA - 15\AA transition and an increase in the temperature of the 15\AA - 12.5\AA transition.

The effect of pressure and temperature on the hydration states of montmorillonite based on our measurements are compared in Fig. 10 with a recently published thermodynamic model proposed by RANSOM and HELGESON (1995). In their model Ransom and Helgeson propose a starting hydration state of 15\AA and a 50% dehydration by approximately 180°C during burial. In contrast, our measurements indicate that the starting hydration state

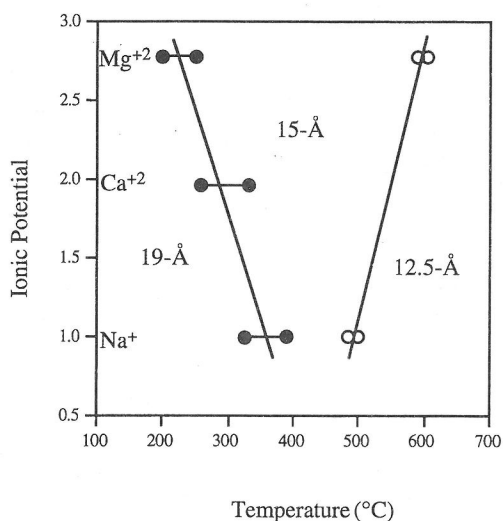


FIG. 9. Plot of the dependence of the 19\AA - 15\AA and 15\AA - 12.5\AA transitions in montmorillonite as a function of ionic potential (ionic charge/radius).

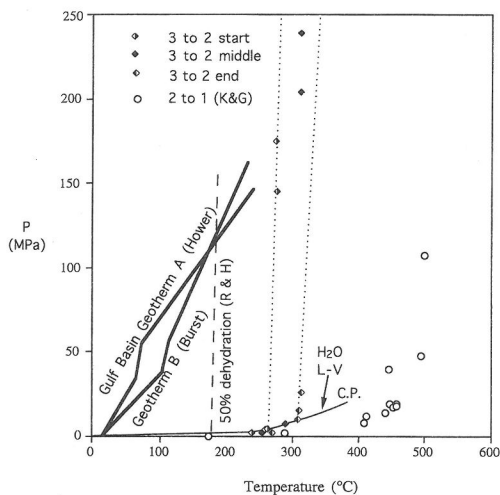


FIG. 10. The two dotted lines bracket our measured dehydration from 19Å to 15Å hydrates and the open circles indicate dehydration from 15Å to 12.5Å hydrates in montmorillonites (KOSTER VANGROOS and GUGGENHEIM, 1987). These data are compared with the recently proposed 50% dehydration (dashed line) assuming an initial 15Å hydrate (RANSOM and HELGESON, 1995). Heavy solid lines show two versions of geotherms from BURST (1969) and HOWER *et al.* (1976).

is 19Å and that dehydration to 15Å does not occur until approximately 200–380°C and the dehydration to the 12.5Å hydrate does not occur until 450–600°C. Thus, our observations indicate that montmorillonite retains more water to higher temperatures than previously thought. These observations are important for sedimentary basin and petroleum generation modeling. Our results indicate that for any water-releasing reaction shallower than 5 km, the 19Å hydrate probably dominates and may be responsible for the release of 44% more water than previously thought. Another consequence of our observations concerns the mechanical properties of montmorillonite clay. Our results show that those clays, if they can escape chemical alteration to illite by potassium, are expected to remain ductile down to considerable depths where they may be the best candidate to form a good seal for deep oil reservoirs.

Our observation that the 15Å hydrate of montmorillonite is stable up to 450–600°C at pressures higher than the H₂O LV curve suggest that clays might be transported down subducting slabs before the remaining water is released. The dehydration in subducting slabs is considered to be an important cause of shallow earthquakes as well as the source of volatiles that create volcanic activity along some of the boundaries of tectonic plates.

CONCLUSIONS

The hydrothermal diamond anvil cell (HDAC) has found a wide variety of applications in the study of geological samples employing a variety of observational techniques where there is need to make observations and measurements at simultaneous high pressure and high temperature. A new paper by CHOU *et al.* (1995), reports the use of the HDAC to study eutectic melting of the assemblage Ca(OH)₂ + CaCO₃ with excess H₂O and lack of evidence for “portlandite II” phase. Another study is under way at the Bayerisches Geoinstitut in Bayreuth, Germany by Spetzler, Shen, and Angel to develop techniques for making ultrasonic velocity measurements as a function of pressure and temperature in the HDAC with gigahertz sound waves. Judging from the interest in the HDAC, many more novel applications will be developed in the years ahead.

Acknowledgements—We wish to thank the Exxon Production Research Company, Houston, TX for supporting the research on clays and organic samples. Some of the research was conducted at the Geophysical Laboratory of the Carnegie Institution of Washington and in US Geological Survey (USGS) research labs. Most of the rest of the technique development and research reported in this paper was supported by diverse grants from the National Science Foundation over a period of several years. We wish to thank the staff of the Cornell High Energy Synchrotron Source for their help in carrying out synchrotron radiation experiments.

REFERENCES

- ALEKSANDROV I. V., GONCHAROV A. F., ZISMAN A. N. and STISHOV S. M. (1987) Diamond at high pressures: Raman scattering of light, equation of state and high pressure scale. *Soviet Phys. JETP* **66**, 384–390.
- BASSETT W. A., SHEN A. H., BUCKNUM M. and CHOU I.-M. (1993) A new diamond anvil cell for hydrothermal studies to 2.5 GPa and from –190 to 1200°C. *Rev. Sci. Instrum.* **64**, 2340–2345.
- BENKHEDDA Z., LANDAIS P., KISTER J., DEREPE J.-M. and MONTHIOUS M. (1992) Spectroscopic analysis of aromatic hydrocarbons extracted from naturally and artificially matured coals. *Energy and Fuels* **6**, 166–172.
- BISMAYER U. and SALJE E. (1981) Ferroelastic phases in Pb₃(PO₄)²-Pb₃(AsO₄)₂; X-ray and optical experiments. *Acta Cryst.* **A37**, 145.
- BURST J. F. (1969) Diagenesis of Gulf Coast clayey sediments and its possible relation to petroleum migration. *Amer. Assoc. Petrol. Geol. Bull.* **53**, 73–93.
- CHOU I.-M., HASELTON H. T., JR., NORD G. L., JR., SHEN A. H. and BASSETT W. A. (1993) Barium titanate as a pressure calibrant in the diamond anvil cell. *Amer. Geophys. Union Trans.* **74**, 170.
- CHOU I.-M. and HASELTON H. T., JR. (1994) Lead titanate as a pressure calibrant in the diamond anvil cell. *Abstr., 16th Gen. Mtng., IMA*, 74–75.
- CHOU, I.-M. and NORD G. L., JR. (1994) Lead phosphate

- as a pressure calibrant in the hydrothermal diamond anvil cell. *GSA Abstr. Progr.* **26**, A-291.
- CHOU I.-M., BASSETT W. A. and BAI T. B. (1995) Hydrothermal diamond anvil cell study of melts: eutectic melting of the assemblage $\text{Ca}(\text{OH})_2 + \text{CaCO}_3$ with excess H_2O and lack of evidence for "portlandite II" phase, *Amer. Mineral.* **80**, 852–853.
- DECKER D. L. and ZHOU Y. X. (1989) Dielectric and polarization measurements on BaTiO_3 at high pressures to the tricritical point. *Phys. Rev. B* **39**, 2432–2438.
- EVANS H. T. JR. (1961) An X-ray diffraction study of tetragonal barium titanate. *Acta Cryst.* **14**, 1019–1026.
- FRANTZ J. D., DUBESSY J. and MYSEN B. O. (1994) Ion-pairing in aqueous MgSO_4 solutions along an isochore to 500°C and 11 kbar using Raman spectroscopy in conjunction with the diamond-anvil cell. *Chem. Geol.* **116**, 181–188.
- HAAR L., GALLAGHER J. S. and KELL G. S. (1984) *NBS/NRC Steam Tables: Thermodynamic and Transport Properties and Computer Programs for Vapor and Liquid States of Water in SI Units*. Hemisphere Publ. Corp., Washington D. C., 320 pp.
- HANDFLAND M., SYASSEN K., FAHY S., LOUIS S.G. and COHEN M. L. (1985) Pressure dependence of first-order Raman mode in diamond. *Phys. Rev. B* **31**, 6896–6899.
- HERCHEN H. and CAPPELLI M. A. (1991) First-order Raman spectrum of diamond at high temperatures. *Phys. Rev. B* **43**, 11740–11744.
- HOWER J. E., HOWER M. E. and PERRY E. A. (1976) Mechanism of burial metamorphism of agillaceous sediments. I. mineralogical and chemical evidence, *Geol. Soc. Amer. Bull.* **87**, 725–737.
- KOSTER VAN GROOS, A. F. and GUGGENHEIM, S. (1987) Dehydration of Ca- and Mg-exchanged montmorillonite (SWy-1) at elevated pressure. *Amer. Mineral.* **72**, 292–298.
- LIN R. and RITZ G. P. (1993) Studying individual macerals using I.R. microspectroscopy and implications on oil versus gas/condensate proness and "low-rank" generation: *Org. Geochem.* **20**, 695–706.
- MATTHIAS B. (1948) The growth of barium titanate crystals. *Phys. Rev.* **73**, 808–809.
- MIRWALD P. W. and MASSONNE H.-J. (1980) The low-high quartz and quartz-coesite transition to 40 kbar between 600°C and 1600°C and some reconnaissance data on the effect of NaAlO_2 component on the low quartz-coesite transition. *J. Geophys. Research* **85**, 6983–6990.
- MUINOV M. H., KANDA H. and STISHOV S. M. (1994) Raman scattering in diamond at high pressure: isotope effects. *Phys. Rev. B* **50**, 13860–13862.
- RAMIREZ R., LAPENA M. F. and GONZALO J. A. (1990) Pressure dependence of free-energy expansion coefficients in PbTiO_3 and BaTiO_3 and tricritical-point behavior. *Phys. Rev. B* **42**, 2604–2606.
- RANSOM B. and HELGESON H. (1995) A chemical and thermodynamic model of dioctahedral 2:1 layer clay minerals in diagenetic processes: dehydration of dioctahedral aluminous smectite as a function of temperature and depth in sedimentary basins. *Amer. J. Sci.* **295**, 245–281.
- RITZERT V. G. and FRANCK E. U. (1968) Elektrische Leitfähigkeit wässriger Lösungen bei hohen Temperaturen und Drücken, I. KCl , BaCl_2 , $\text{Ba}(\text{OH})_2$, und MgSO_4 bis 750°C und 6 kbar. *Ber. Bunsenges. Phys. Chem.* **72**, 798–808.
- SAMARA G. A. (1971) Pressure and temperature dependence of the dielectric properties and phase transitions of the ferroelectric perovskites: PbTiO_3 and BaTiO_3 . *Ferroelectrics.* **2**, 277–289.
- SAUL A., DUBESSY J. and WAGNER W. (1989) A fundamental equation of water covering the range from the melting line to 1273 K at pressures up to 25000 MPa. *J. Phys. Chem. Ref. Data* **18**, 1537–1565.
- SCHIFERL D., SHARMA S. K., COONEY T. F., WANG S. Y. and MOHANAN K. (1993) Multichannel Raman spectroscopy system for weakly scattering materials at simultaneous high pressures and high temperatures. *Rev. Sci. Instrum.* **64**, 2821–2827.
- SCHIFERL D., SHARMA S. K., COONEY T. F., WANG S. Y., ANTHONY T. R. and FLEISCHER J. F. (in preparation). The use of the diamond $\text{C}^{13}/\text{C}^{12}$ isotope Raman sensor system at high temperatures and pressures for aqueous and other chemically reactive environments.
- SHARMA S. K., MAO H. K., BELL P. M. and XU J. A. (1985) Measurement of stress distribution in diamond anvils with micro-Raman spectroscopy. *J. Raman Spectrosc.* **16**, 350–352.
- SHARMA S. K., COONEY T. F. and WANG S.Y. (1994) Structure of alkali-silicate and germania glasses at high temperature and pressure. *J. Non-Cryst. Solids* **179**, 125–134.
- SHEN A. H., BASSETT W. A. and CHOU I.-M. (1992) Hydrothermal studies in a diamond anvil cell: Pressure determination using the equation of state of H_2O . In *High-Pressure Research: Application to Earth and Planetary Sciences* (eds. Y. SYONO and M. H. MANGHANI), 61–68. Terra Sci. Pub. Co./ AGU, Tokyo/Washington, D.C.
- SHERMAN W. F. (1985) The diamond Raman band as a high pressure calibrant. *J. Phys. C* **18**, L973–L978.
- TARDIEU A., CANSELL F. and PETITET J. P. (1990) Pressure and temperature dependence of first-order Raman mode of diamond. *J. Appl. Phys.* **68**, 3243–3245.
- VAN VALKENBURG A., BELL P. M. and MAO H. K. (1987) High-pressure mineral solubility experiments in the diamond-window cell In *Hydrothermal Experimental Techniques* (eds. G. C. ULMER and H. L. BARNES), pp. 458–468. J. Wiley and sons, New York
- WAGNER W., SAUL A. and PRUSS A. (1994) International equations for the pressure along the melting and along the sublimation curve of ordinary water substance. *J. Phys. Chem. Ref. Data* **23**, 515–527.
- ZOUBOULIS E. S. and GRIMSDITCH M. (1991) Raman scattering in diamond up to 1900 K. *Phys. Rev. B* **43**, 12490–12493.